Acta Astronautica 123 (2016) 376–386

Contents lists available at ScienceDirect

Acta Astronautica

journal homepage: www.elsevier.com/locate/actaastro

Faster-than-natural spacecraft circumnavigation via way points

Trevor Bennett [a], Hanspeter Schaub [a], Christopher W.T. Roscoe [b]

[a] University of Colorado, Boulder, CO 80309, USA
[b] Applied Defense Solutions, Columbia, MD 21044, USA

ARTICLE INFO

Article history:
Received 19 August 2015
Received in revised form
5 January 2016
Accepted 29 January 2016
Available online 6 February 2016

Keywords:
Forced circumnavigation
Way point navigation
Relative motion control
Maneuver effort prediction

ABSTRACT

Circumnavigation relative motion is considered for applications such as inspecting a space object for damage, or characterizing space debris before engaging a remediation operation. Faster-than-natural circumnavigation is a guidance method in which the deputy spacecraft is advanced ahead of the natural Keplerian relative motion. A state transition matrix method of generating a discrete way point guidance solution is proposed for faster-than natural circumnavigation. The state transition matrix methodology is applied to both circular and elliptical chief orbits. For the circular chief case, natural relative trajectories are planar in nature. With the faster-than-natural circumnavigation, this work illustrates how the required relative trajectories become three-dimensional curves. This methodology allows for closed-form impulsive control solutions and the associated fuel cost. Numerical simulations illustrate and validate the proposed method.

1. Introduction

Circumnavigation orbits are useful for inspection type missions, formation flying science and Earth observation, engaging in servicing missions, or even performing the proposed electrostatic tugging and formations [1]. The limitation of these circumnavigation relative orbits is that the natural motion solutions require one orbit period to complete. Further, the natural motion solutions may not provide the relative way points needed by the deputy satellite to obtain the desired relative orbit. A variety of methods exist for relative orbit control for missions such as PRISMA, TerraSAR-X, and the Magnetospheric Multiscale Mission [2–5]. A wide range of relative orbit formulations and control methodologies exist for such missions; however, this study considers an impulsive approach to relative motion control through prescribing relative orbit way points and desired flight time.

This study utilizes the state transition matrix formulation to perform faster-than-natural circumnavigation via a set of pre-defined way points. Several authors have explored the faster-than-natural relative orbits providing initial insight into continuous thrusting solutions. Ref. [6] investigates using a bi-elliptic method to find a 2-impulse sequence to join 2 natural elliptic relative motions, yielding a faster-than-natural circumnavigation. Straight uses the relative motion state transition matrix (STM) for the circular chief case to develop impulsive control solutions to yield a non-natural circular circumnavigation solution [7]. Here a general set of way points can be applied to both circular and elliptical chief orbits, and the STM is used to determine the required changes in velocity at each way point. Ref. [8] also uses the circular chief STM to investigate using a series of way points to perform a faster-than-natural approach to another space object. STM methods that scale to elliptic

E-mail addresses: trevor.bennett@colorado.edu (T. Bennett), hanspeter.schaub@colorado.edu (H. Schaub), croscoe@applieddefense.com (C.W.T. Roscoe).

http://dx.doi.org/10.1016/j.actaastro.2016.01.025
0094-5765/

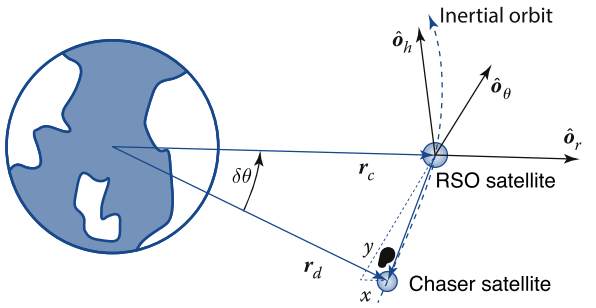

Fig. 1. Local vertical local horizontal rotating frame for formation flying. [12].

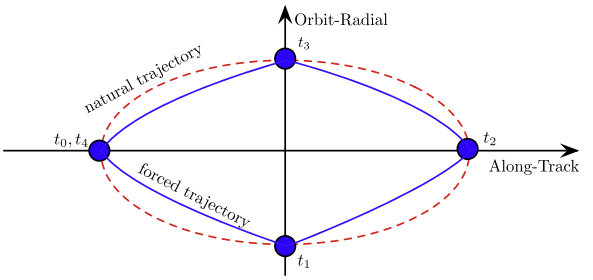

Fig. 2. Illustration of relative motion way points.

orbits are investigated in Ref. [9]. More recently, Dannemiller discusses the general STM approach to planning a multi-maneuver relative trajectory in Ref. [10].

Faster-than-natural circumnavigation presents additional flexibility in the design of formation flying relative orbits. The STM-based approach provides opportunities for discrete guidance solutions with impulsive maneuvers. Consider two spacecrafts in formation in the rotating local vertical local horizontal (LVLH) frame defined in Fig. 1. Given the Keplerian orbits of the two spacecrafts, the relative orbit of the deputy spacecraft remains constant and bounded. This paper investigates a method of advancing the deputy spacecraft to discrete points along the natural relative orbit in a faster time than otherwise feasible with the natural uncontrolled propagation of Keplerian motion. The concept of faster-than-natural circumnavigation is illustrated by the forced trajectory shown in Fig. 2. The natural relative motion for the deputy spacecraft, under the assumption of Keplerian orbits, follows the dotted red trajectory around the chief spacecraft. Applying precise Δv maneuvers at way points, shown as blue points, enables the deputy spacecraft to reach the subsequent way point at a prescribed time denoted as t_i earlier than otherwise possible. The time reduction to complete the faster-than-natural circumnavigation is captured in a unitless speed up factor.

The application of faster-than-natural circumnavigation for both circular and elliptical chief orbits is investigated. In this study the Keplerian relative motion STM is developed based on the orbit element difference approach to be generally applicable. Of interest is the maneuver cost and time benefit from a non-natural relative orbit period while requiring the satellite still visit targeted way points of the naturally occurring relative trajectory. The naturally occurring relative orbits are planar, and the impact of changing the way point visit time on the relative trajectory is investigated. Alfriend and Gim develop the relative motion STM in Ref. [11] assuming both point-mass and J_2 gravitational influences, even if eccentric chief motions is considered. In this paper, as control solutions implement non-natural relative trajectories, the impact of the J_2 perturbation is assumed to be minimal between two impulsive control burns. While this study utilizes a simplified Alfriend and Gim STM formulation, the general methodology is applicable to any system accompanied by an STM. The simplified Gim/Alfriend STM is useful in developing analytical fuel consumption predictions over considered chief eccentricity with variable speed up factor cases. Further, the approach scales to elliptic chief motions as well. While closed form solutions are feasible, their analytical expressions can be rather lengthy. The faster-than-natural way point navigation is explored in simple two way point scenario with a highly eccentric chief to provide the elliptical chief insight with available simplifications. The impact of the eccentric chief motion on the inter-way point trajectories is investigated both in the geometrical distortion of the relative orbit and in the maneuver cost required. The influence of both the speed up factor and eccentricity are considered. Relative motion with an eccentric chief becomes quick complex. The goal of this study is to show how the presented methodology can be applied to eccentric chief cases, and highlight some interesting challenges that arise with non-zero eccentricities. Numerical simulations are used to demonstrate the resulting solutions.

2. Circumnavigation way points

This study examines how a deputy spacecraft performs relative orbit maneuvers such that resulting circumnavigation is either faster or slower than the natural relative orbit period. The maneuver sequence is set up through a series of N_{wp} way points relative to the chief satellite as shown in Fig. 2. The illustration shows a 2D in-plane relative trajectory; however, these way points can also contain out of plane z components. For simplicity in this study, uniform time segments are assumed between way points. If $P = \frac{2\pi}{n}$ is the natural relative motion period with mean motion n, then $T \leq P$ is the period required to circumnavigate through these way points. The time between way points is distributed uniformly such that the elapsed time of each segment is

$$T_i = \frac{T}{N_{\text{wp}}} \tag{1}$$

The time T_i for circular chief motion represents an intuitive geometrical division of the relative orbit. As is seen in later sections, equal segment time does not necessarily correspond to equal geometrical spacing. The deputy circumnavigation time will be less than the natural period prescribed by the speed up factor $0 < s < \infty$ such that

$$s = \frac{P}{T} \tag{2}$$

The speed up factor provides the natural motion for $s=1$, slower than natural for $s < 1$, and faster-than-natural for

$s > 1$. The sped up time between way points is expressed in terms of the chief mean orbital motion n and the number of way points N_{wp} as

$$T_i = \frac{2\pi}{nN_{wp}s} \tag{3}$$

Intuitively, increasing the speed up factor requires more ΔV. Also, the spacing of way points influences the ΔV budget. The influence from both the speed up and number of way points is addressed in later sections.

The time between way points is defined by the desired speed up factor. The relative motion is propagated and studied using the circular chief state transition matrix (STM) for the deputy spacecraft between way point maneuvers. Utilizing ΔV_i maneuvers at the way points between STM coast periods completes the faster-than-natural circumnavigation. The uniform spacing of the way points simplifies the following analysis, however the methodology is applicable to non-uniform way point spacing. The methodology is also expanded to an elliptical chief case presented in later sections.

3. Relative motion state transition matrix

The ΔV budget can be expressed analytically given the prescribed relative orbit and speed up factor. The motion can be propagated through the use of a state transition matrix that maps the current deputy position forward in time assuming Keplerian motion. The STM further provides the required relative position and velocity state of the deputy at the respective way points given the sequence of maneuvers. This is achieved by first allowing the relative motion state vector to be

$$\boldsymbol{X} = [x \;\; y \;\; z \;\; \dot{x} \;\; \dot{y} \;\; \dot{z}]^T = \left[\boldsymbol{r}^T \;\; \boldsymbol{v}^T\right]^T \tag{4}$$

The state transition matrix $[\Phi_{\boldsymbol{X}}(t,t_0)]$ maps initial $\boldsymbol{X}(t_0) = \boldsymbol{X}_0$ states into the current states $\boldsymbol{X}(t)$ at time t through

$$\boldsymbol{X}(t) = [\Phi_{\boldsymbol{X}}(t,t_0)]\boldsymbol{X}_0 \tag{5}$$

An elegant analytical solution to the STM is available when derived from orbit elements. Consider the semi-non-singular orbit element set [12]

$$\mathcal{oe} = \{a, \theta, i, q_1, q_2, \Omega\} \tag{6}$$

where a is the semi-major axes, $\theta = \omega + f$ is the true latitude with the argument of periapse ω, true anomaly f, the inclination angle i. Defining $q_1 = e\cos\omega$ and $q_2 = e\sin\omega$ as measures of eccentricity e and argument of periapses with Ω as the ascending node angle completes the set.

In formation flying applications, the relative motion is small compared to the orbit radii and the linearized mapping $[A(\mathcal{oe}(t))]$ provides a convenient method to map orbit element differences into the Cartesian LVLH frame position and velocity counter parts [12–14]. The orbit element difference $\delta\mathcal{oe}(t)$ is obtained by differencing the deputy and chief orbit element sets with linearization about the chief element set.

$$\boldsymbol{X}(t) = [A(\mathcal{oe}(t))]\delta\mathcal{oe}(t) \tag{7a}$$

$$\boldsymbol{X}_0 = [A(\mathcal{oe}(t_0))]\delta\mathcal{oe}_0 \tag{7b}$$

The orbit element description has the benefit by assuming Keplerian motion all elements are constant, except for the anomaly measure (θ in the given $\mathcal{oe}$ set). Using the linearized mapping in Eq. (7a), the state transition matrix $[\Phi_{\boldsymbol{X}}]$ can be found using

$$[\Phi_{\boldsymbol{X}}(t,t_0)] = [A(\mathcal{oe}(t))][\Phi_{\delta\mathcal{oe}}(t,t_0)][A(\mathcal{oe}(t_0))]^{-1} \tag{8}$$

The matrix $[A(\mathcal{oe}(t))]$ is defined in parts by [12, pp. 689–690]:

$$[A(\mathcal{oe}(t))] = \begin{bmatrix} A_{11} & A_{12} \\ A_{21} & A_{22} \end{bmatrix} \tag{9a}$$

$$[A_{11}] = \begin{bmatrix} R/a & V_R R/V_T & 0 \\ 0 & R & 0 \\ 0 & 0 & Rs\theta \end{bmatrix} \tag{9b}$$

$$[A_{12}] = \begin{bmatrix} -R(2aq_1 + Rc\theta)/p & -R(2aq_2 + Rs\theta)/p & 0 \\ 0 & 0 & Rci \\ 0 & 0 & -Rc\theta si \end{bmatrix} \tag{9c}$$

$$[A_{21}] = \begin{bmatrix} -V_R/(2a) & (1/R - 1/p)h & 0 \\ -3V_T/(2a) & -V_R & 0 \\ 0 & 0 & V_T c\theta + V_R s\theta \end{bmatrix} \tag{9d}$$

$$[A_{22}] = \begin{bmatrix} (V_R aq_1 + hs\theta)/p & (V_R aq_2 - hc\theta)/p & 0 \\ (3V_T aq_1 + 2hc\theta)/p & (3V_T aq_2 + 2\,hs\theta)/p & V_R ci \\ 0 & 0 & (V_T s\theta - V_R c\theta)si \end{bmatrix} \tag{9e}$$

where the short-hand notation $c\theta = \cos\theta$ and $s\theta = \sin\theta$ is used, along with the definitions

$$R = r = \frac{a(1 - q_1^2 - q_2^2)}{1 + q_1 c\theta + q_2 s\theta} \tag{10a}$$

$$V_R = \frac{h}{p}(q_1 s\theta - q_2 c\theta) \tag{10b}$$

$$V_T = \frac{h}{p}(1 + q_1 c\theta + q_2 s\theta) \tag{10c}$$

$$p = a(1 - e^2) \tag{10d}$$

$$h = \sqrt{\mu p} \tag{10e}$$

Here the orbit has semi-major axis a and eccentricity e about the central body with gravitational parameter μ. The inverse of $[A(\mathcal{oe}(t))]$ is taken to obtain $[A(\mathcal{oe}(t))]^{-1}$ with analytical solution in Ref. [14].

The orbit element description has the benefit of assuming Keplerian motion where all orbit elements are constant except for the anomaly measure (θ in the given $\mathcal{oe}$ set). Thus, the state transition matrix for the differential

orbit elements $\delta\mathcal{OE}$ assumes the simple form [12, p. 697]

$$[\Phi_{\delta\mathcal{OE}}(t,t_0)]=\begin{bmatrix}1&0&0&0&0&0\\A&B&0&C_1&C_2&0\\0&0&1&0&0&0\\0&0&0&1&0&0\\0&0&0&0&1&0\\0&0&0&0&0&1\end{bmatrix} \tag{11}$$

where

$$A=-\frac{3}{2}\frac{a\eta}{r^2}nt \tag{12a}$$

$$B=\left(\frac{r_0}{r}\right)^2 \tag{12b}$$

$$\begin{aligned}C_1=&\frac{1}{r^2\eta^2}\big(rs\theta(r+a(1-q_1^2))-r_0s\theta_0(r_0+a(1-q_1^2))\\&+aq_1q_2(rc\theta-r_0c\theta_0)+q_2(r-r_0)(a+r+r_0)\big)\\C_2=&\frac{1}{r^2\eta^2}\big(-rc\theta(r+a(1-q_2^2))+r_0c\theta_0(r_0+a(1-q_2^2))\\&-aq_1q_2(rs\theta-r_0s\theta_0)-q_1(r-r_0)(a+r+r_0)\big)\end{aligned} \tag{12c}$$

using the following definitions in terms of $\mathcal{OE}$:

$$\eta=\sqrt{1-q_1^2-q_2^2} \tag{13}$$

$$r=\frac{a\eta^2}{1+q_1\cos\theta+q_2\sin\theta} \tag{14}$$

$$r_0=\frac{a\eta^2}{1+q_1\cos\theta_0+q_2\sin\theta_0} \tag{15}$$

Note that this solution to $[\Phi_{\delta\mathcal{OE}}]$ assumes that $\theta(t)$ is found separately by solving Kepler's equation. For circular chief motion, the implementation of Kepler's equation reduces simply to the change in time at a mean motion as analogous to change in angle. The more complicated inclusion of time of flight is discussed in the specific derivation of the elliptical chief motion. Therefore, the state transition matrix $[\Phi_{\boldsymbol{X}}]$ can be found using

$$[\Phi_{\boldsymbol{X}}(t,t_0)]=[A(t)][\Phi_{\delta\mathcal{OE}}(t,t_0)][A(t_0)]^{-1} \tag{16}$$

Using the linearized mapping in Eq. (7a) and extensive algebraic simplification of Eq. (8) provides the state transition matrix for general spacecraft motion. This methodology applies generally to Keplerian linearized relative motion. The only restriction to the presented methodology is that the inclination angle must be non-zero, $i\neq 0$, because of the cot$i$ in the inverse of $[A(\mathcal{OE}(t))]$. However, this constraint is irrelevant when $i=0$ is set in $[A(\mathcal{OE}(t))]$ before inversion as is done for circular chief relative motion and the planar relative motion discussed in the elliptical chief development.

Utilizing the analytical form of the state transition matrix, we can solve for the next way point position $\boldsymbol{r}_{i+1}$ in terms of the current way point position $\boldsymbol{r}_i$ and the corresponding departure velocity $\boldsymbol{v}_i^+$ using impulsive burns.

$$\boldsymbol{r}_{i+1}=[\Phi_{\boldsymbol{X},11}(t_{i+1},t_i)]\boldsymbol{r}_i+[\Phi_{\boldsymbol{X},12}(t_{i+1},t_i)]\boldsymbol{v}_i^+ \tag{17}$$

Given the $\boldsymbol{r}_i$ and $\boldsymbol{r}_{i+1}$ way point information, this can be solved for the current way point desired open-loop departure velocity $\boldsymbol{v}_i^+$ using

$$\boldsymbol{v}_i^+=[\Phi_{\boldsymbol{X},12}(t_{i+1},t_i)]^{-1}\left(\boldsymbol{r}_{i+1}-[\Phi_{\boldsymbol{X},11}(t_{i+1},t_i)]\boldsymbol{r}_i\right) \tag{18}$$

where $[\Phi_{\boldsymbol{X},12}(t_{i+1},t_i)]^{-1}$ maps the position error back to the present state. Applying the impulsive burn, the expected arrival velocity at the next way point is given by

$$\boldsymbol{v}_{i+1}^-=[\Phi_{\boldsymbol{X},21}(t_{i+1},t_i)]\boldsymbol{r}_i+[\Phi_{\boldsymbol{X},22}(t_{i+1},t_i)]\boldsymbol{v}_i^+ \tag{19}$$

Thus, the open-loop burn $\Delta\boldsymbol{v}_i$ at the ith way point is given by

$$\Delta\boldsymbol{v}_i=\boldsymbol{v}_i^+-\boldsymbol{v}_i^- \tag{20}$$

with the total ΔV budget as the sum of all way point burn magnitudes. Considered in the following sections are three implementations of the proposed methodology. First presented is the circular chief case with both four and two way point solutions. Following is the elliptic chief case results using two way points.

4. Circular chief circumnavigation

The simplest relative orbit to consider first is the motion around a circular chief. Significant simplification of Eq. (8) is possible using $r\to a$, $r_0\to a$, and with zero eccentricity $q_1\to 0$, and $q_2\to 0$. The resulting STM for linearized motion around a circular chief is [15]

$$[\Phi_{\boldsymbol{X}}]=\begin{bmatrix}\Phi_{\boldsymbol{X},11}&\Phi_{\boldsymbol{X},12}\\\Phi_{\boldsymbol{X},21}&\Phi_{\boldsymbol{X},22}\end{bmatrix} \tag{21a}$$

$$[\Phi_{\boldsymbol{X},11}]=\begin{bmatrix}4-3\cos(nt)&0&0\\6(\sin(nt)-nt)&1&0\\0&0&\cos(nt)\end{bmatrix} \tag{21b}$$

$$[\Phi_{\boldsymbol{X},12}]=\begin{bmatrix}\frac{\sin(nt)}{n}&\frac{2(1-\cos(nt))}{n}&0\\-\frac{2(1-\cos(nt))}{n}&\frac{4\sin(nt)}{n}-3t&0\\0&0&\frac{\sin(nt)}{n}\end{bmatrix} \tag{21c}$$

$$[\Phi_{\boldsymbol{X},21}]=\begin{bmatrix}3n\sin(nt)&0&0\\-6n(1-\cos(nt))&0&0\\0&0&-n\sin(nt)\end{bmatrix} \tag{21d}$$

$$[\Phi_{\boldsymbol{X},22}]=\begin{bmatrix}\cos(nt)&2\sin(nt)&0\\-2\sin(nt)&4\cos(nt)-3&0\\0&0&\cos(nt)\end{bmatrix} \tag{21e}$$

Recall that in the circular chief case, the change in the anomaly angle is $\Delta f=\Delta M=nt$. The change in the angle is easily obtained from Kepler's equation for any point-to-point state transition in a circular orbit. Therefore the simplification $\Delta f=nt=\alpha$ is employed enabling any point-to-point transition. The constant $[\Phi_{\boldsymbol{X},ij}]$ state transition submatrices are then simplified to

$$[\Phi_{\boldsymbol{X},11}]=\begin{bmatrix}4-3\cos(\alpha)&0&0\\6(\sin(\alpha)-\alpha)&1&0\\0&0&\cos(\alpha)\end{bmatrix} \tag{22a}$$

$$\left[\Phi_{\boldsymbol{X},12}\right]=\begin{bmatrix}\frac{\sin(\alpha)}{n} & \frac{2(1-\cos(\alpha))}{n} & 0\\ -\frac{2(1-\cos(\alpha))}{n} & \frac{4\sin(\alpha)}{n}-\frac{3\alpha}{n} & 0\\ 0 & 0 & \frac{\sin(\alpha)}{n}\end{bmatrix} \tag{22b}$$

$$[\Phi_{\boldsymbol{X},21}]=\begin{bmatrix}3n\sin(\alpha) & 0 & 0\\ -6n(1-\cos(\alpha)) & 0 & 0\\ 0 & 0 & -n\sin(\alpha)\end{bmatrix} \tag{22c}$$

$$[\Phi_{\boldsymbol{X},22}]=\begin{bmatrix}\cos(\alpha) & 2\sin(\alpha) & 0\\ -2\sin(\alpha) & 4\cos(\alpha)-3 & 0\\ 0 & 0 & \cos(\alpha)\end{bmatrix} \tag{22d}$$

The following algorithm makes use of the inverse of $[\Phi_{\boldsymbol{X},12}]$. The analytical inverse solution is given as

$$[\Phi_{\boldsymbol{X},12}]^{-1}=\frac{1}{\kappa}\begin{bmatrix}n(3\alpha-4\sin\alpha) & 2n(1-\cos\alpha) & 0\\ -2n(1-\cos\alpha) & -n\sin\alpha & 0\\ 0 & 0 & \kappa n\csc\alpha\end{bmatrix} \tag{23}$$

with

$$\kappa=8\cos\alpha+3\alpha\sin\alpha-8 \tag{24}$$

The analytical form for the open loop Δv enables fuel and time cost analysis and enables parameter tuning. Visualization of these results is presented in the following sections.

5. Simulated 4 way point study

Simulation of the open-loop Δv computation provides visualization of the faster-than-natural circumnavigation concept. Consider the circular chief case where $N_{\text{wp}}=4$ with $A_0>0$ and $B_0>0$. In the current study the way points are assumed to have even temporal spacing throughout the maneuver. The maneuver time T_i between way points is given in Eq. (3). Assuming a general number N_{wp} of way points leads to

$$t=T_i=\frac{1}{n}\underbrace{\frac{2\pi}{N_{\text{wp}}s}}_{\alpha}=\frac{\alpha}{n} \tag{25}$$

For the specific case where $N_{\text{wp}}=4$, then

$$\alpha=\frac{\pi}{2s} \tag{26}$$

The motion between the way points is computed using the STM mapping

$$\boldsymbol{X}(t)=[\Phi_{\boldsymbol{X}}(t,t_i)]\boldsymbol{X}(t_i)\quad\forall\, t_i<t<t_{i+1} \tag{27}$$

The faster-than-natural circumnavigation study focuses on the open-loop impulsive burns where Eq. (5) is also used to generate the reference motion. The presented form in Eq. (27) allows for any reference motion to be prescribed from any set of initial relative orbit conditions. This form is also employed in the elliptic chief case.

A variety of relative orbits are available for study. Considered here is a generic 2-1 planar ellipse with an equivalent radial and normal component magnitude. The mean motion of the chief is fixed at $n=0.0007$ rad/s. The considered four way point positions are given in sequence by

$$\boldsymbol{r}(t_0)=-2A_0\hat{\boldsymbol{o}}_\theta \tag{28a}$$

$$\boldsymbol{r}(t_1)=-A_0\hat{\boldsymbol{o}}_r-B_0\hat{\boldsymbol{o}}_h \tag{28b}$$

$$\boldsymbol{r}(t_2)=+2A_0\hat{\boldsymbol{o}}_\theta \tag{28c}$$

$$\boldsymbol{r}(t_3)=A_0\hat{\boldsymbol{o}}_r+B_0\hat{\boldsymbol{o}}_h \tag{28d}$$

$$\boldsymbol{r}(t_4)=-2A_0\hat{\boldsymbol{o}}_\theta \tag{28e}$$

The prescribed points reside on the nominal trajectory. Enforced are the endpoint velocities to start from and end on the nominal relative orbit.

$$\boldsymbol{v}(t_0^-)=\boldsymbol{v}(t_0^+)=-nA_0\hat{\boldsymbol{o}}_r-nB_0\hat{\boldsymbol{o}}_h \tag{29}$$

The "$-$" super-script indicates the LVLH frame velocity prior to a burn, and the "$+$" super-script indicates the post-burn LVLH frame velocity.

Provided an analytical expression for the STM in Eq. (22a), desired is the total ΔV required to perform a particular faster-than-natural circumnavigation. To simplify the following descriptions, the two parameter definitions are introduced

$$\beta_1=1-\sin\alpha-\cos\alpha \tag{30a}$$

$$\beta_2=1+\sin\alpha-\cos\alpha \tag{30b}$$

The analytical prediction for the four way point ΔV utilizes the definition in Eq. (20). The analytical ΔV requirement at each way point is tabulated in Table 1 for the prescribed way point sequence in Eq. (28a). To evaluate the total fuel cost, the $\Delta\boldsymbol{v}_i$'s about all body axes are summed using

$$\Delta v_{\text{total}}=\sum_{i=0}^{N_{\text{wp}}}|\Delta\boldsymbol{v}_i\cdot\hat{\boldsymbol{o}}_r|+|\Delta\boldsymbol{v}_i\cdot\hat{\boldsymbol{o}}_\theta|+|\Delta\boldsymbol{v}_i\cdot\hat{\boldsymbol{o}}_h| \tag{31}$$

Using the analytical form in Table 1, the total Δv simplifies to

$$\begin{aligned}\Delta v_{\text{total}}=&\frac{2A_0n}{|\kappa|}(4|\beta_1|+2|4\beta_1+3\alpha\cos(\alpha)|+|3\alpha+4\beta_1\\&-3\alpha\sin(\alpha)|)+2B_0n(|\cot(\alpha)|+|1-\csc(\alpha)|)\end{aligned} \tag{32}$$

The particular multi-burn circumnavigation strategy is implemented in Mathematica. The speedup factor is set to $s=1.7$ for faster-than-natural and $s=0.75$ for slower-than natural. The relative orbit parameters are set to $A_0=B_0=10$ meters. The resulting relative motion is illustrated in Fig. 3

Table 1
Analytical $\Delta\boldsymbol{v}_i$ Burn Solution for a 4-Way point Circumnavigation Maneuver.

Time	$\Delta\boldsymbol{v}_i\cdot\hat{\boldsymbol{o}}_r$	$\Delta\boldsymbol{v}_i\cdot\hat{\boldsymbol{o}}_\theta$	$\Delta\boldsymbol{v}_i\cdot\hat{\boldsymbol{o}}_h$
t_0	$\frac{A_0n}{\kappa}(3\alpha\sin(\alpha)-3\alpha-4\beta_1)$	$\frac{2A_0n\beta_1}{\kappa}$	$-B_0n\csc\alpha$
t_1	$\frac{2A_0n}{\kappa}(4\beta_1+3\alpha\cos\alpha)$	0	$2B_0n\cot\alpha$
t_2	0	$-\frac{4A_0n\beta_1}{\kappa}$	0
t_3	$-\frac{2A_0n}{\kappa}(4\beta_1+3\alpha\cos\alpha)$	0	$-2B_0n\cot\alpha$
t_4	$\frac{A_0n}{\kappa}(3\alpha\sin(\alpha)-3\alpha-4\beta_1)$	$\frac{2A_0n\beta_1}{\kappa}$	$B_0n\csc\alpha$

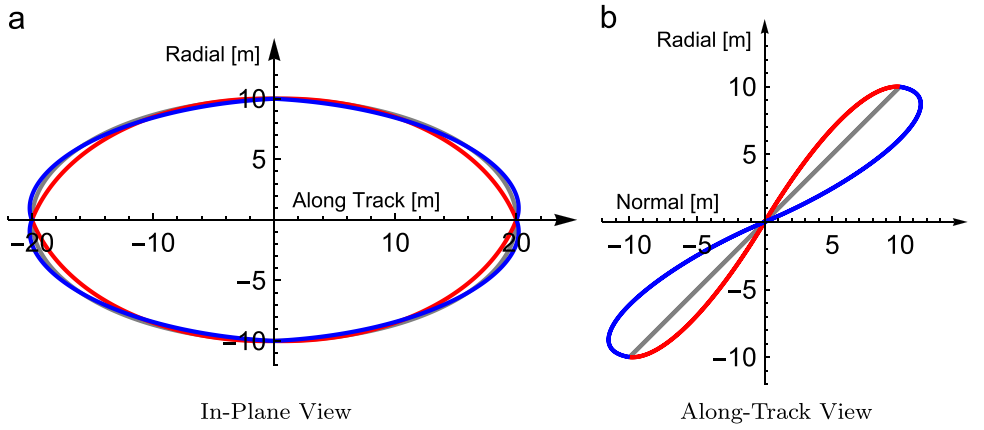

Fig. 3. Open-loop forced four way point circumnavigation Illustration using $A_0 = B_0 = 10$ meters. (—- $s=1.7$, —- $s=0.75$, –– natural motion).

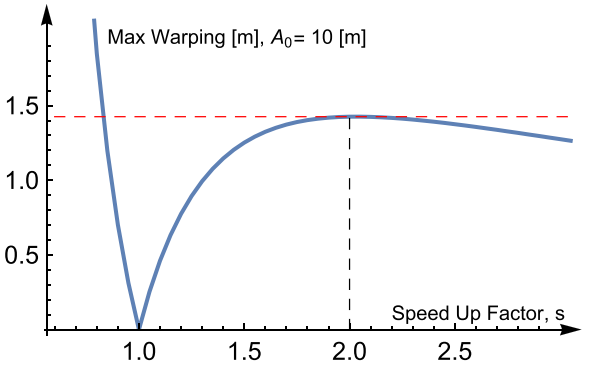

Fig. 4. Maximum warping away from the nominal circumnavigation plane.

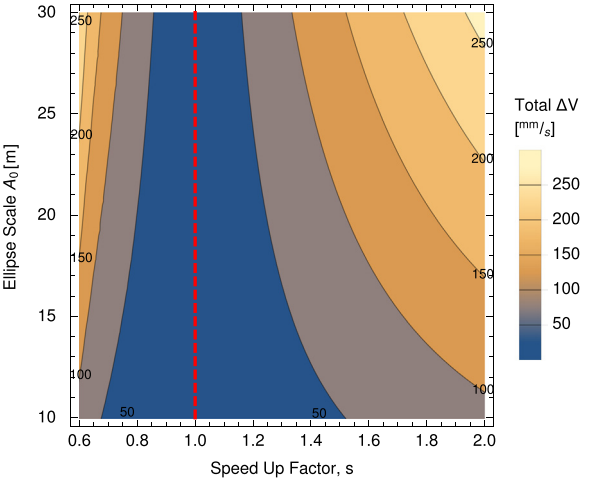

Fig. 5. Total ΔV for the four way point circular chief. Nominal is shown by —-.

with nominal in grey. Fig. 3 does not provide clear visualization of the inertial transfer orbits to transition between way points. However, it does provide significant insight into the warping of the relative motion required for faster-than-natural circumnavigation. The in-plane projection in Fig. 3(a) shows that the sped up circumnavigation shown in red requires sharper trajectory changes at the way points on the along-track axis. The along-track view in Fig. 3(b) shows that in order to meet the out-of-plane way points, the relative motion is not longer a planar curve, but rather a three-dimensional curve. The planar view in Fig. 3(a) exhibits the expected squeeze in the relative motion plane. More interestingly, the along-track view in Fig. 3(b) reveals the true warping. The slower than natural motion warps in the opposite manner to the faster-than-natural motion. The planar motion seen in Fig. 3 (a) shows that the relative motion expands with the local velocity at each way point driving the spacecraft out away from the nominal. The along-track view in Fig. 3(a) shows how the spacecraft shifts largely out-of-plane to delay the arrival.

Sweeping through the speed up factors above unity reveals that the maximum warping of the along-track view occurs with $s=2$. This is evidenced in Fig. 4. The value $s=2$ physically describes a series of transfer orbits that phase the deputy spacecraft by half a period. As expected with the circular chief, the faster-than-natural relative motion is symmetric. This symmetry breaks down for the elliptic chief case. Increasing the speed up factor such that $s>2$ transitions the relative orbit geometry towards hyperbolic point-to-point trajectories. This manifests an along-track view warping that decreases back into the nominal plane. The slower-than-natural solutions, $s<1$, exhibit an exponential divergence from the nominal relative orbit as the new trajectory approaches the infinite size relative orbit at $s=0$.

The decrease in speed up factor from unity introduces a greater sensitivity in geometry change and ΔV requirement than does the increase in speed up factor. This is evidenced in Fig. 5 where variations in the speed up factor and relative orbit sizing are considered. The nominal $s=1$ does not require any burns and is marked with the dashed red line. The asymmetry in speed up factor and the increased requirement for larger orbits are visible in Fig. 5. Consistent with the more substantial relative orbit change seen in Fig. 3 for the slower circumnavigation, Fig. 5 highlights the more rapidly increasing ΔV requirement for the same increment of change in the speed up factor. Recall that the speed up factor appears in the denominator of the time of flight. It is therefore expected that

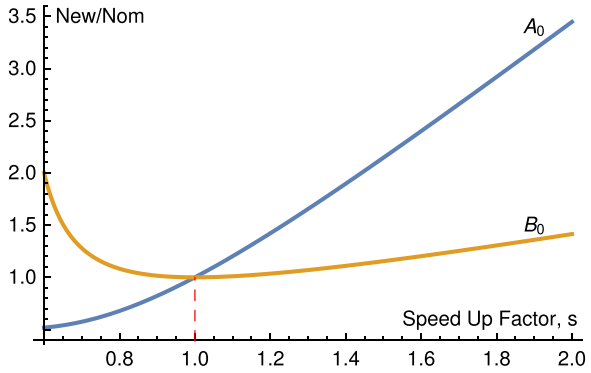

Fig. 6. Open-loop forced four way point circumnavigation CW parameter distortion.

decreasing s towards zero will have an inverse power increase in ΔV with an inverse power decrease towards larger speed up factors. Further exhibited is the increase in ΔV as the geometry enlarges. This is as expected as greater distance reduction is required for larger geometries with the same speed up factor.

The geometric change in the relative orbit is further visualized by inspecting the change in the Clohessy-Wiltshire (CW) parameters as a function of the speed up factor. Recall the general form of the CW equations, as shown in Eq. (33a), which provide the relative motion of a deputy satellite as a function of time and constant parameters [16].

$$x(t) = A_0 \cos(nt+\alpha) + x_{\text{off}} \tag{33a}$$

$$y(t) = -2A_0 \sin(nt+\alpha) - \frac{3}{2} nt x_{\text{off}} + y_{\text{off}} \tag{33b}$$

$$z(t) = B_0 \cos(nt+\beta) \tag{33c}$$

The parameters A_0 and B_0 prescribe the elliptical size of the relative motion whereas the x_{off} and y_{off} prescribe the offsets and drift. The distortion of the typical elliptical shape seen in Fig. 3 appears when either the relative motion is sped up or slowed down. The alteration to the relative motion is further illustrated by mapping the change into the CW parameter space.

Solving for the inverse mapping of the CW equations in Eq. (33a) transforms the LVLH frame state into a CW parameter state. The inverse mapping assumes the form

$$A_0 = \frac{\sqrt{9n^2x^2 + \dot{x}^2 + 12nx\dot{y} + 4\dot{y}^2}}{n} \tag{34a}$$

$$\alpha = \tan^{-1}\left(\frac{\dot{x}}{-3nx - 2\dot{y}}\right) - nt \tag{34b}$$

$$B_0 = \frac{\sqrt{n^2z^2 + \dot{z}^2}}{n} \tag{34c}$$

$$\beta = \tan^{-1}\left(\frac{-\dot{z}}{nz}\right) - nt \tag{34d}$$

$$x_{\text{off}} = 4x + 2\frac{\dot{y}}{n} \tag{34e}$$

$$y_{\text{off}} = -2\frac{\dot{x}}{n} + y + (6nx + 3\dot{y})t \tag{34f}$$

Using the inverse mapping, the sped up way points are mapped into the CW parameter values. The distortion in these parameters, and therefore the geometrical distortion, is shown in Fig. 6 for the ellipse sizing and Fig. 7 for the offsets.

Decreasing the speedup factor towards zero introduces an asymptotic divergence of the elliptical scaling parameters as visible in Fig. 6. Using a speedup factor of 0.6, the far left in Fig. 6 shows the A_0 parameter tending towards zero as the B_0 tends toward infinite. This physically represents the distortion seen in Fig. 3(b) where the out of plane motion tends towards an arc with increasing magnitude perpendicular to the nominal relative orbit plane. The A_0 parameter shrinks towards zero allowing a drift towards the way points with the offset parameters.

The offset parameters are shown in Fig. 7(a) and (b), respectively. The offset parameters take on 2 values: the first half from way point 0 to way point 2 and the second half going from way point 2 to way point 4. The significance is that the CW parameterized relative motion has an offset and drift that characterizes faster-than-natural motion. There is no discontinuity in the value for the offsets through a particular relative orbit. Inserting impulsive maneuvers in the LVLH frame introduces new velocity components into the inverse mapping to the CW parameters. The impulsive maneuver at the midpoint of the relative motion, way point 2 in this case, provides the change in offset and drift required.

An example of a circular chief faster-than-natural circumnavigation via way points is presented. Given the trajectory magnitudes considered, Fig. 5 demonstrates the speed up is feasible with less than 250 mm/s. The following sections introduce the elliptic chief case and another circular chief case used for comparison.

6. Circular 2 way point study to compare with an elliptic chief

The more general form for faster-than-natural circumnavigation is desired to enable implementations with an elliptic chief. As mentioned in the derivation of the state transition matrix form, the elliptic chief does not have a linear relationship between time of flight and true anomaly change. Therefore, the elliptic chief way points are set to periapse and apoapse for simplicity in the STM although the proposed methodology applies generally.

Consider first a comparison case where the chief is held circular and only the periapse and apoapse way points are used: a true anomaly of 0 and π for the circular chief. Utilizing the decoupling in the natural relative orbit, the out-of-plane motion is removed to provide isolation of the eccentric influence on planar relative motion. The mean motion of the chief is fixed at $n=0.0007$ rad/s and the considered two way point positions are given in sequence by

$$\boldsymbol{r}(t_0) = -2A_0\hat{\boldsymbol{o}}_\theta \tag{35a}$$

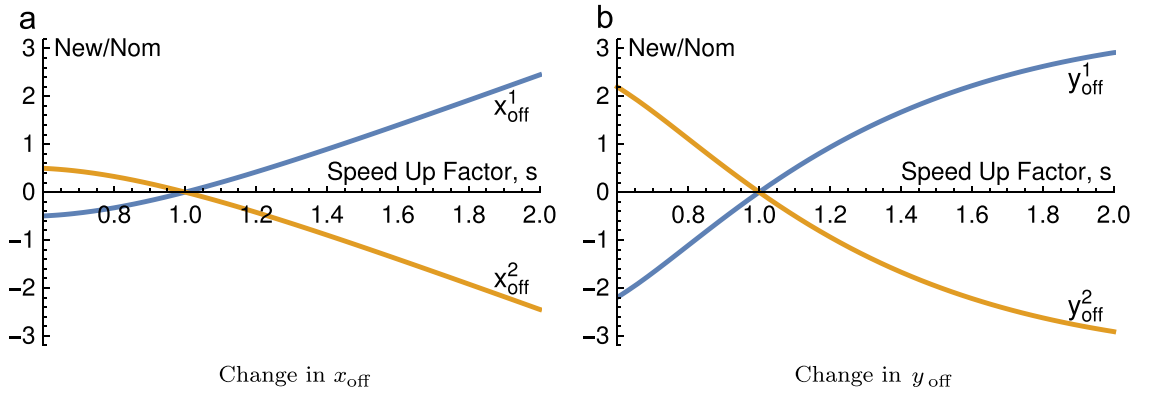

Fig. 7. Open-loop forced four way point circumnavigation CW parameter distortion.

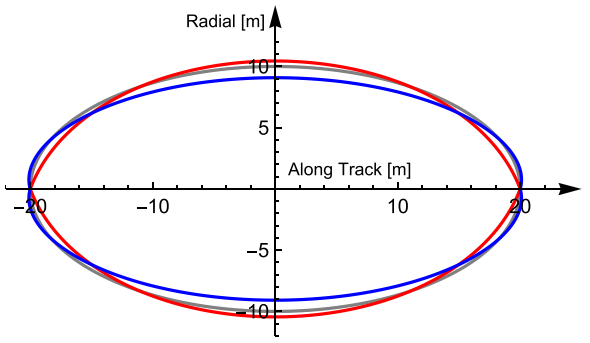

Fig. 8. Open-loop forced two way point circumnavigation using $A_0 = 10$ and $B_0 = 0$ m. (—- $s=1.7$, —- $s=0.75$, —- Natural Motion).

$$\boldsymbol{r}(t_1) = +2A_0\hat{\boldsymbol{o}}_\theta \tag{35b}$$

$$\boldsymbol{r}(t_2) = \boldsymbol{r}(t_0) \tag{35c}$$

Again, enforced are the endpoint velocities to start from and end on the nominal relative orbit.

$$\boldsymbol{v}(t_0^-) = \boldsymbol{v}(t_0^+) = -nA_0\hat{\boldsymbol{o}}_r \tag{36}$$

Similar to the development employed in Table 1, an analytical expression for the two way point circular chief ΔV is available and is not included here. The prescribed nominal relative motion and the relative orbits with a speed up factors of $s=1.7$ and $s=0.75$ are shown in Fig. 8. Unlike the planar motion seen in Fig. 3(a), the faster circumnavigation traverses outside of the nominal trajectory at the most radial nodes. The relaxation of the way points down from 4 to 2 moves the circumnavigation closer to the efficiency of a 2-burn phasing maneuver. The important feature in Fig. 8 is that the relative motion remains symmetric for each segment with the circular chief.

The reduced ΔV requirements are characterized in Fig. 9. The respective ΔV magnitudes have diminished in comparison to Fig. 5. Comparison of Figs. 5 and 9 demonstrates the trend towards the more efficient 2-burn phasing solution.

The circular chief examples are fully presented with comparisons drawn between two and four way point solutions. The proposed faster-than-natural circumnavigation STM methodology is again applied to an elliptic

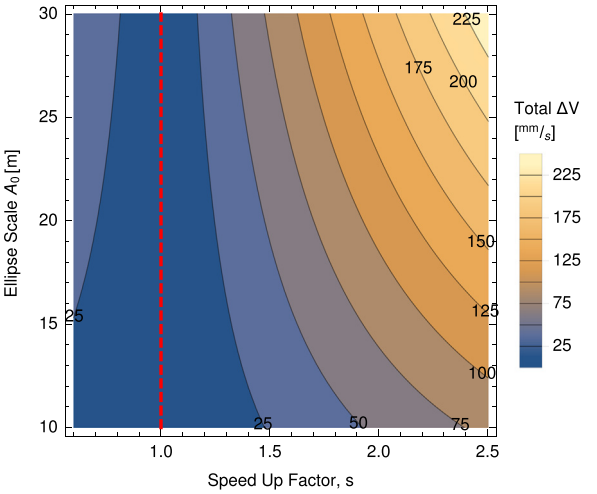

Fig. 9. Total ΔV for the two way point circular chief. Nominal is shown by —.

chief. The results of the circular chief sections provide examples for comparison to develop insight into the influence of ellipticity.

7. Elliptical chief STM development

Given the circular chief cases presented, the elliptical chief case can be considered and compared. The prescription of the relative orbit fundamentally changes in moving to an elliptic chief. Consider the conceptual visualization of the faster-than-natural circumnavigation with an elliptic chief shown in Fig. 10. The nominal way points are placed at the periapse and apoapse locations with respective LVLH frames. While two way points are selected for the present elliptical chief study, the methodology applies generally to any number of way points. The true anomaly for the nominal relative motion propagates from 0 to π for the first segment and π to 2π for the second segment. The faster-than-natural circumnavigation advances the relative orbit way points to an earlier true anomaly. The red LVLH frames shown in Fig. 10 represent the new relative motion coordinate systems at the advanced true anomaly positions.

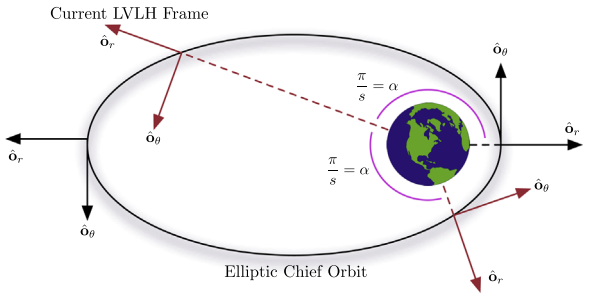

Fig. 10. Speed up factor influence on the positions of the way points for the elliptic chief.

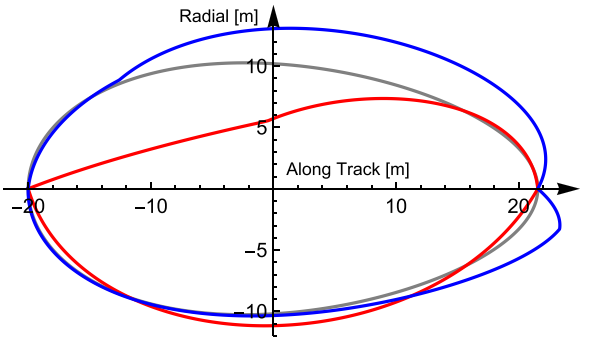

Fig. 11. Open-loop forced two way point circumnavigation using $A_0 = 10$ meters. (—- $s=1.7$, —- $s=0.88$, –- Natural Motion).

Also seen in Fig. 10 is the two part propagation through $\Delta f = \pi/s$ which is fundamental to the STM construction.

The required STMs for both the circular and elliptical chiefs are constructed from the Eq. (8). In the circular chief case, the time of flight and the change in anomaly angle were linearly related. In the eccentric chief, the time of flight and true anomaly change are not linearly related. Further, in Eq. (10a) the gravitational parameter μ and the semi-major axis a appear in the STM. The equations can be non-dimensionalized by introducing the mean motion $n = \sqrt{\mu/a^3}$. The resulting elliptic chief STM retains terms of the form nt. The time of flight t can be removed from the STM by inserting the geometrical change provided by Kepler's equation. Recall, the time-of-flight for a spacecraft under 2-Body motion is expressed by Kepler's equation

$$M(t) = M_0 + n(t - t_0) \tag{37}$$

Given that the desired faster-than-natural circumnavigation requires a mapping to the true anomaly speed-up, the definition of the eccentric anomaly from the mean anomaly is utilized

$$M(t) = E(t) - e\sin(E(t)) \tag{38}$$

Further, the eccentric anomaly is related to the true anomaly through

$$\tan\left(\frac{E(t)}{2}\right) = \sqrt{\frac{1-e}{1+e}}\tan\left(\frac{f(t)}{2}\right) \tag{39}$$

The time of flight $t - t_0$ is therefore obtained by inserting Eq. (38) into Eq. (37) with the definitions in Eq. (39). The use of Kepler's equation dictates that a single general STM cannot be applied to all segments for the elliptic chief trajectory. That is, a unique STM is constructed for each segment. In the case of the two way point solution, the respective STMs employed are

$$\left[\Phi_{\boldsymbol{X},1}\left(f=\frac{\pi}{s}, f_0=0\right)\right] \quad \left[\Phi_{\boldsymbol{X},2}\left(f=\frac{2\pi}{s}, f_0=\frac{\pi}{s}\right)\right] \tag{40}$$

The speed up factor is present in the elliptic STMs such that the midpoint maneuver happens at a shifted true anomaly. Effectively, the speed up factor advances the true anomaly of the relative orbit geometry. The second state transition matrix $[\Phi_{\boldsymbol{X},2}]$ may often span across the chief apoapse and introduces substantial relative motion influence for the later half of the trajectories considered.

For the following visualizations, the chief eccentricity is set to a modest $e=0.3$ with a mean motion of $n=0.0007$ rad/s. The argument of periapse is set to zero and the inclination of the chief orbit does not appear in the planar relative orbit case. The considered two way point positions are given in sequence by

$$\boldsymbol{r}(t_0) = -2A_0\hat{\boldsymbol{o}}_\theta \tag{41a}$$

$$\boldsymbol{r}(t_1) = [\Phi_{\boldsymbol{X},1}(f=\pi, f_0=0)]\boldsymbol{X}(t_0) \approx +2.2A_0\hat{\boldsymbol{o}}_\theta \tag{41b}$$

$$\boldsymbol{r}(t_2) = \boldsymbol{r}(t_0) \tag{41c}$$

The nominal velocity conditions enforced are the endpoint velocities.

$$\boldsymbol{v}(t_0^-) = \boldsymbol{v}(t_0^+) = -nA_0\hat{\boldsymbol{o}}_r \tag{42}$$

The prescribed nominal relative motion and the relative orbits with a speed up factor of $s=1.7$ and speed of $s=0.88$ are shown in Fig. 11. The first segment of the faster-than-natural trajectory appears to have similar form to the segments seen in the circular chief. As anticipated, the second part of the relative motion segment experiences dramatically different character than the circular chief. Most notable is the turn inward well inside the near 2–1 nominal ellipse. Recall that the trajectory begins in a trailing along-track position and then transitions into the negative radial towards the leading along track position. A critical set of features in Fig. 11 are the kinks in the relative motion trajectory. These kinks are indicative of apoapse and periapse crossings. Careful inspection of the first segment in the slower than natural trajectory reveals a kink at the largest along-track magnitude. Utilizing a speed up factor of $s=0.88$ dictates that the first way point is reached after the chief has passed through apoapse. The trajectory kink marks the chief apoapse crossing. Observe the most clear kink in the second half of the slower than natural trajectory in Fig. 11 where the trajectory nearly aligns with the nominal. The slowed trajectory reaches the second way point, or the original relative position, after the chief has passed periapse. The chief periapse crossing introduces this kink. Careful inspection reveals that a kink also exists in the faster-than-natural trajectory just following the second segment crossing a zero along-track position. This kink event marks the chief apoapse crossing for the faster-than-natural circumnavigation.

The effect of an elliptic chief is evidenced in the kinked relative motion trajectories for faster-than-natural circumnavigation. The behavior is further examined with a sweep of speed

up factors ranging over $s_{min} = 1.1$ to $s_{max} = 1.9$ with an increment of $\Delta s = 0.2$. The collection of trajectories is displayed in sweeping color shown in Fig. 12. Careful inspection of Fig. 12 reveals the chief apoapse crossing in all trajectories. As expected, the larger the speed up the later in the second segment the kink appears.

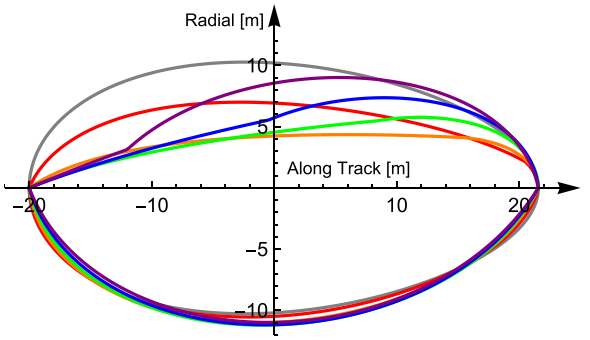

Fig. 12. Open-loop forced two way point circumnavigation using $A_0 = 10$ and $B_0 = 0$ meters. (—- $s = 1.1$, —- $s = 1.3$, —- $s = 1.5$, —- $s = 1.7$, —- $s = 1.9$, —- Natural Motion).

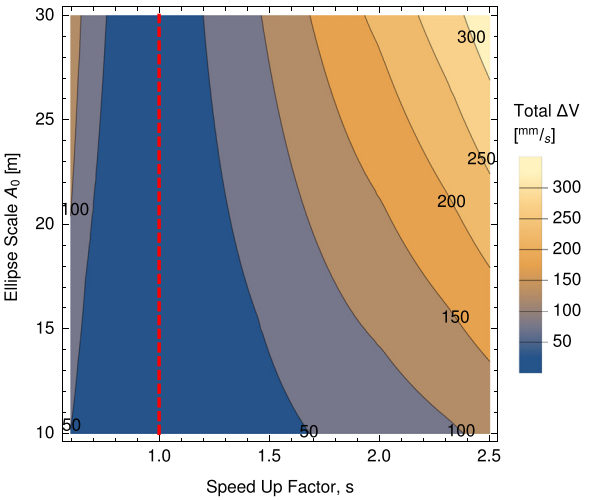

Fig. 13. Total ΔV for the two way point elliptic chief. Nominal is shown by - - - - line.

The behavior in Fig. 12 influences the ΔV requirement sweep with clear speed up markers. Fig. 13 presents a sweep of the speed up factor and initial position geometry. Inspection of $s=2$ in Fig. 13 reveals a kink transition in the smooth contour. The physical significance of the $s=2$ vertical is that speed up factors greater than 2 never cross the chief apoapse. An increasing negative slope is present immediately following the $s=2$ vertical suggesting a discontinuity in efficiency change for such transfers. Comparison of Fig. 13 and the circular chief case in Fig. 9 shows that the elliptic chief relative orbit requires greater ΔV for the same speed up factor and semi-major axis. This is largely attributed to the nonlinear time of flight and maneuver efficiency change due to eccentricity experienced by the deputy around and elliptic chief. To effect the same speed up change, a greater ΔV than the circular counterpart is required.

The influence of the chief eccentricity is highly nonlinear in the total maneuver cost. Explored in Fig. 14 is the total ΔV required for a two way point faster-than-natural circumnavigation as a function of chief eccentricity and speed up factor. Fig. 14 presents 2 ranges of speed up factor to provide clarity over the more heavily considered region of $0.5 \leq s$ and an additional presented region of $\frac{1}{6} \leq s \leq 0.5$. Interestingly, the maneuver cost for large speed up factors is least near an eccentricity of $e=0.5$. The nonlinear maneuver cost contours demonstrate the complexity of the eccentric chief problem.

Important solutions exist for particular speed up factors in the implementation of faster-than-natural circumnavigation. Not clearly visible in Fig. 13 are the ΔV contours for $s=0.5$ which represents way points that double the period of the deputy spacecraft orbit. In the presented elliptical chief two way point solution, a speed up factor $s=0.5$ is equivalent to a 2-1 resonant orbit where the same final phasing is obtained by not performing any way point maneuvers. The integer resonance is seen in Fig. 14 where the 3-1 resonance is zero-cost at $s = \frac{1}{3}$, the 4-1 resonance is

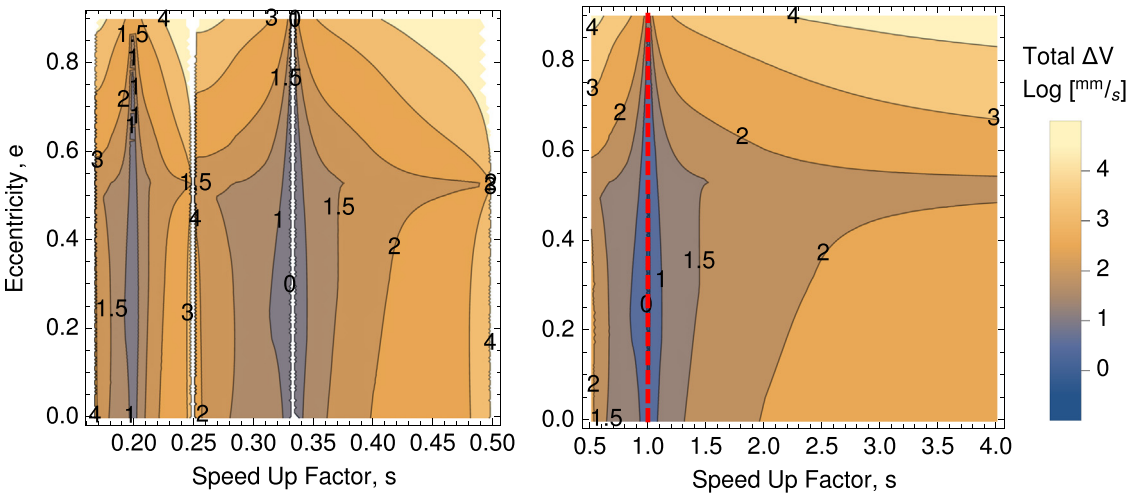

Fig. 14. Two way point elliptic chief total ΔV versus eccentricity and speed up factor.

zero-cost at $s=\frac{1}{4}$, and the integer fraction $s=\frac{1}{k}$ for $k=1,2,3,\ldots$ capturing all the resonance orbits. While all the resonant orbit speed up factors will equate to a zero-cost solution with no speed up, the presented results in Fig. 14 show a repeating character of the cost contours between $s=\frac{1}{2k}$ speed up factors. This is believed to be the result of formulating a two way point solution.

A selected case of the elliptic chief faster-than-natural circumnavigation is presented although the formulation is generally applicable for a variety of eccentricities and speed up factors. The maneuver cost analysis of the proposed STM methodology is demonstrated for general faster-than-natural circumnavigation reconfigurations. In addition, the STM solution is equipped to address the multi-revolution solutions, phasing with a speed up of $s<0.5$, for either the circular or elliptic chief. The proposed methodology is also applicable to formulations involving any number of way points. The presented study provides the methodology and several implementations of the proposed faster-than-natural circumnavigation technique to reveal some of the insights and complexities. As seen in Fig. 14, the effect of eccentricity is nonlinear motivating future study of alternate numbers of way points and elliptical chief maneuver cost predictions.

8. Conclusions

The development and demonstration for impulsive faster-than-natural circumnavigation solutions applied to general relative orbit geometries. The general relative motion state transition matrix is derived from an orbit-element difference formulation for both the circular and elliptic chief cases. Two cases are shown of circular chief faster-than-natural circumnavigation and one case of an elliptic chief. The results demonstrate how the natural relative orbit trajectory warps into a three-dimensional curve off of the nominal if the circumnavigation time is sped up or slowed down. A maximum three-dimensional warping is found to occur around a speed up factor of 2 for the circular chief case. As the speed up factor is further increased, the non-planar warping is reduced back towards the nominal plane. Further, for the elliptic chief case, the way point matching may result in more complex relative trajectories due to the periapse and apoapse regions. As shown, the total maneuver cost increases with an increase in speed up factor with more nonlinear cost behavior influenced by eccentricity. Future work will consider a greater range of elliptical chief cases and will consider eccentric anomaly, mean anomaly, and/or direct orbit element difference formulations.

Acknowledgements

The authors would like to thank the NASA Space Technology Research Fellowship (NSTRF) program, grant number NNX14AL62H, for support of this research. Further, we thank Jason Westphal from Applied Defense Solutions for his discussions on this topic.

References

[1] E. Hogan, H. Schaub, Space debris reorbiting using electrostatic actuation, AAS Guidance and Control Conference, Breckenridge, CO, February 3–8, 2012, Paper AAS 12–016.
[2] S. Persssonn, B. Jakobsson, E. Gill, PRISMA demonstration mission for advanced rendezvous and formation flying technologies and sensors, in: 56th International Astronautical Congress, October, 2005.
[3] S. Persson, S. Veldman, P. Bodin, PRISMA? A formation flying project in implementation phase, Acta Astronaut. 65 (9–10) (2009) 1360–1374.
[4] R. Werninghaus, S. Buckreuss, The TerraSAR-X mission and system design, IEEE Trans. Geosci. Remote Sens. 48 (February (2)) (2010) 606–614.
[5] S. Curtis, The Magnetospheric multiscale mission. . .resolving fundamental processes in space plasmas, Report of the NASA Science and Technology Definition Team for the MMS Mission, NASA/TM-2000-209883, 1999.
[6] Y. Masutani, M. Matasushita, F. Miyazaki, Flyaround maneuvers on a satellite orbit by impulsive thrust control, in: Proceedings of the 2001 IEEE International Conference on Robotics & Automation, Vol. 1, 2001, pp. 421–426, http://dx.doi.org/10.1109/ROBOT.2001.932587.
[7] S.D. Straight, Maneuver design for fast satellite circumnavigation (Master's thesis), Air Force Institute of Technology, March 2004.
[8] W. Zhou, J. Yuan, J. Luo, Flying robots fast circumnavigation trajectory design and guidance, in: IEEE International Conference on Robotics and Biomimetics, December 2006, pp. 263–267, http://dx.doi.org/10.1109/ROBIO.2006.340164.
[9] J.-j. Luo, W.-y. Zhou, J.-p. Yuan, A general method of trajectory design and guidance for fast satellite circumnavigation, J. Astronaut. 3 (2007) 628–632.
[10] D.P. Dannemiller, Multi-Maneuver Clohessy-Wiltshire Targeting, in: AAS/AIAA Astrodynamics Specialist Conference, Girdwood, Alaska, July 31–August 4, 2011, Paper AAS 11–650.
[11] D.-W. Gim, K.T. Alfriend, The state transition matrix of relative motion for the perturbed non-circular reference orbit, AIAA J. Guid. Control Dyn. 26 (6) (2003) 956–971.
[12] H. Schaub, J.L. Junkins, Analytical Mechanics of Space Systems, 2nd ed., AIAA Education Series, Reston, VA, October 2009.
[13] H. Schaub, K.T. Alfriend, Hybrid cartesian and orbit element feedback law for formation flying spacecraft, AIAA J. Guid. Control Dyn. 25 (March–April) (2002) 387–393.
[14] K.T. Alfriend, H. Schaub, D.-W. Gim, Gravitational perturbations, nonlinearity and circular orbit assumption effect on formation flying control strategies, in: Proceedings of the Annual AAS Rocky Mountain Conference, Breckenridge, CO, February 2–6, 2000, pp. 139–158.
[15] D.A. Vallado, Fundamentals of Astrodynamics and Applications. Microcosm Press, El Segundo, California, 4th ed., March 2013.
[16] W.H. Clohessy, R.S. Wiltshire, Terminal guidance system for satellite rendezvous, J. Aerosp. Sci. 27 (September) (1960) 653–658.